



CHORUS

This is the accepted manuscript made available via CHORUS. The article has been published as:

Accurate Determination of Blackbody Radiation Shifts in a Strontium Molecular Lattice Clock

B. Iritani, E. Tiberi, W. Skomorowski, R. Moszynski, M. Borkowski, and T. Zelevinsky
Phys. Rev. Lett. **131**, 263201 — Published 26 December 2023

DOI: [10.1103/PhysRevLett.131.263201](https://doi.org/10.1103/PhysRevLett.131.263201)

Accurate Determination of Blackbody Radiation Shifts in a Strontium Molecular Lattice Clock

B. Iritani^{1,*}, E. Tiberi^{1,*}, W. Skomorowski², R. Moszynski³, M. Borkowski^{1,4,5,†} and T. Zelevinsky^{1,‡}

¹*Department of Physics, Columbia University, 538 West 120th Street, New York, NY 10027-5255, USA*

²*Centre of New Technologies, University of Warsaw, Banacha 2c, 02-097 Warsaw, Poland*

³*Quantum Chemistry Laboratory, Department of Chemistry, University of Warsaw, Pasteura 1, 02-093 Warsaw, Poland*

⁴*Van der Waals-Zeeman Institute, Institute of Physics, University of Amsterdam, Science Park 904, 1098 XH Amsterdam, The Netherlands*

⁵*Institute of Physics, Faculty of Physics, Astronomy and Informatics, Nicolaus Copernicus University, Grudziadzka 5, 87-100 Torun, Poland*

(Dated: November 21, 2023)

Molecular lattice clocks enable the search for new physics, such as fifth forces or temporal variations of fundamental constants, in a manner complementary to atomic clocks. Blackbody radiation (BBR) is a major contributor to the systematic error budget of conventional atomic clocks and is notoriously difficult to characterize and control. Here, we combine infrared Stark-shift spectroscopy in a molecular lattice clock and modern quantum chemistry methods to characterize the polarizabilities of the Sr₂ molecule from dc to infrared. Using this description, we determine the static and dynamic blackbody radiation shifts for all possible vibrational clock transitions to the 10⁻¹⁶ level. This constitutes an important step towards mHz-level molecular spectroscopy in Sr₂, and provides a framework for evaluating BBR shifts in other homonuclear molecules.

Frequency standards are the cornerstone of precision measurement. Optical atomic clocks set records in both precision and accuracy, and are poised to redefine the second [1–7]. There is a growing interest in precision measurements with molecules [8–12]. The simple structure of homonuclear diatoms like Sr₂ makes them ideal testbeds to probe new physics, including searching for corrections to gravity at short distances [13–16] and temporal variation of fundamental constants [12, 17–26]. Thus, there is interest in improving techniques for molecular spectroscopy. Even for ultra-precise atomic clocks, the blackbody radiation (BBR) shift remains a primary contribution to the uncertainty of the clock measurement [3, 4, 27–32], and is notoriously difficult to control and characterize [33–35]. State-of-the-art evaluations of BBR shift rely on measurements of the differential dc polarizability of the clock states in conjunction with modeling of dynamic contributions [36–40].

Previously, we demonstrated record precision and accuracy for a molecular lattice clock by measuring a 32-THz transition between two vibrational levels in ultracold Sr₂ molecules, reaching a 4.6×10^{-14} systematic uncertainty [41]. Estimates of the BBR contribution to this uncertainty relied on preliminary theoretical modelling of polarizabilities that lacked experimental verification. Here, we determine room-temperature BBR shifts for our molecular clock to the 10⁻¹⁶ level. To do so, we employ modern quantum chemistry methods to determine the differential polarizabilities for all vibrational clock transitions and verify our theory directly by measuring Stark shifts induced by a mid-infrared laser for a wide variety of molecular clock transitions (Fig. 1). Given this combined experimental and theoretical picture, we develop a complete description of the BBR effect for all vibrational levels within the ground-state potential of ⁸⁸Sr₂ molecules.

The experimental sequence closely follows that of our previous works [9, 41–43]. A 2- μ K sample of ultracold stron-

tium atoms is trapped in a one-dimensional, horizontal, near-infrared optical lattice. We form weakly bound molecules via a photoassociation pulse tuned to the -353-MHz 1_u resonance [44]. This bound state predominantly decays to a pair of rotational $J = 0, 2$ states of the top vibrational state, $v' = 62$, in the ground-state potential. We then apply a two-photon Raman pulse to probe selected clock transitions. We detect the number of remaining $v' = 62$ molecules by photodissociation [45] and counting the recovered atoms. Unless otherwise specified, we always refer to rotationless $J = 0$ states in the electronic ground-state potential, and list the lower energy state first for a given transition, regardless of where the molecular population is initialized.

We rely on narrow-linewidth Raman transitions between the least bound $v' = 62$ vibrational state and selected deeply bound vibrational states v [Fig. 1(a)]. We address each of these transitions via intermediate states v'' in the electronically excited $(1)0_u^+$ potential. The vibrational splittings are determined by the difference in the pump ($v' \rightarrow v''$) and anti-Stokes ($v'' \rightarrow v$) laser frequencies. We select intermediate states with favorable Franck-Condon factors for the pump and anti-Stokes transitions for each interrogated pair of clock states (Table I). We address clock states throughout the potential well using three different intermediate states in the excited $(1)0_u^+$ potential: $v'' = 11$ [at -57 084 156.51(12) MHz from the ¹S₀+³P₁ threshold], $v'' = 15$ [at -48 855 512.13(18) MHz], and $v'' = 16$ [at -47 036 433.95(23) MHz]. The selection of intermediate states is a balancing act between available lasers and transition strengths, and required several diode lasers in the 727–735 nm and 760–800 nm wavelength ranges.

We locate the vibrational states v using Autler-Townes spectroscopy: we first induce molecular loss with the pump laser, and then scan the anti-Stokes laser until the line is split into a doublet [43, 46–50]. While high-precision absolute de-

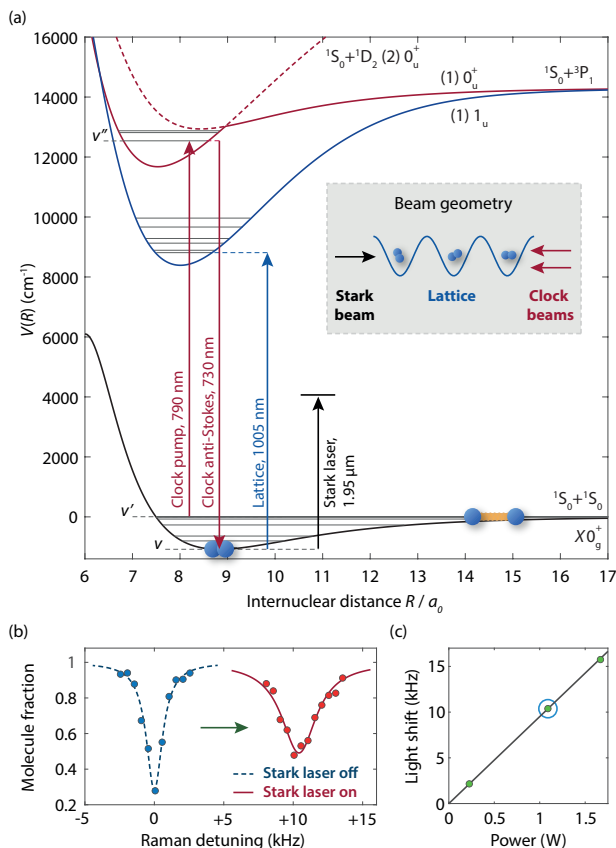


FIG. 1. Stark-shift spectroscopy in Sr_2 on the example $0 \leftrightarrow 62$ transition. (a) We rely on narrow two-photon Raman transition via an intermediate state in the $(1)0_u^+$ (red arrows) in a magic lattice that couples the deeply-bound clock state v to an excited $(1)1_u$ state (blue arrow). (b) We induce Stark shifts to probe differential polarizabilities of ground ro-vibrational states with $1.95 \mu\text{m}$ light. (c) Example light shift measurement. The encircled point corresponds to subplot (b).

terminations of these binding energies are beyond the scope of this Letter, we list the vibrational splittings $f_{v \leftrightarrow v'}$ to <100 kHz (Table I). The uncertainty is fully dominated by light shifts [51].

By employing several strategies to achieve 1-kHz spectroscopic resolution, we can determine ac Stark shifts to ~ 150 Hz using Lorentzian fits (Supplemental Material). After initially locating the transitions, we switch to a Raman configuration by detuning $+30$ MHz from the intermediate resonance to narrow down our transition linewidth. We stabilize the pump laser to a high finesse ($>3 \times 10^5$) cavity using a Pound-Drever-Hall lock [53, 54], which in turn provides a stable reference for the repetition rate of an optical frequency comb. We then lock our anti-Stokes clock laser to the frequency comb. This locking scheme ensures the stability of the frequency difference between the two Raman lasers. In addition to stabilizing our clock lasers, we rely on magic trapping to reduce inhomogeneous broadening. Our method utilizes polarizability crossings generated by the dispersive behavior of the target

state polarizability near transitions to the electronically excited $(1)1_u$ potential [9]. We select $(1)1_u$ states such that the line strength S [42] is greater than $\sim 10^{-5} (ea_0)^2$ (here e is the electron charge, a_0 is the Bohr radius). Large line strengths correspond to large magic detunings, allowing few-ms molecular lifetimes, and Fourier-limited linewidths of 1 kHz or better. Our lattice laser is wavemeter-locked to ~ 30 MHz precision.

To determine differential polarizabilities we induce ac Stark shifts on these clock transitions using an additional $1.95 \mu\text{m}$ laser. We typically observe ac Stark shifts of up to 20 kHz [as shown for $0 \leftrightarrow 62$ in Fig. 1(b)]. We measure ac Stark shifts of each transition as a function of $1.95 \mu\text{m}$ laser power relative to the $27 \leftrightarrow 62$ transition [Fig. 1(c)]. We do not observe any significant hyperpolarizability [41] and therefore we fit a simple proportion. To determine the differential polarizability, we need to adequately characterize the intensity of the $1.95 \mu\text{m}$ light at our molecules. To do so, we compare the ac Stark shift of the $27 \leftrightarrow 62$ transition to that of the $\Delta m = 0$ component of atomic intercombination $^1S_0 \rightarrow ^3P_1$ transition with a differential polarizability of $+326.2(3.6)$ a.u. [55]. For our maximum power of 1.7 W, we have an intensity of 6.8 kW/cm^2 . For most transitions, this scheme allows us to determine the differential polarizabilities to 5% as listed in Table I and shown in Fig. 2. Any thermal shifts stemming from our $5\text{-}\mu\text{K}$ sample [56] are negligible (Supplemental Material).

To calculate the BBR shifts we need a model of the differential polarizabilities at all wavelengths from dc to infrared. The overwhelming majority of the BBR spectrum falls below $2 \mu\text{m}$. While we cannot experimentally probe this entire range of wavelengths, we can leverage close agreement between theory and experiment at $1.95 \mu\text{m}$ and extend theoretical models to provide a full description of the BBR shift. We use modern quantum chemistry methods to calculate the differential

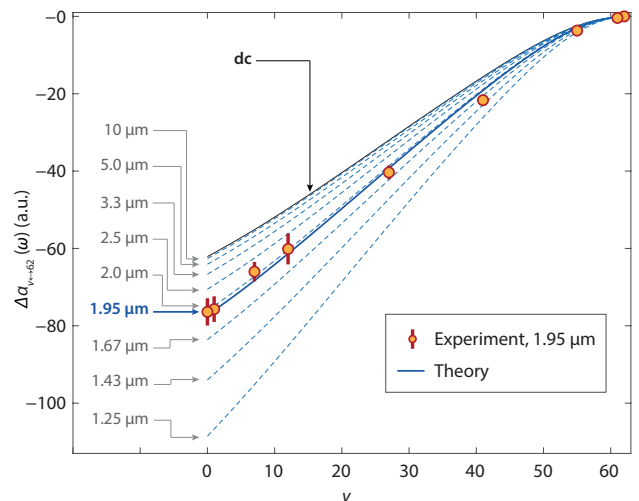


FIG. 2. Differential polarizability with respect to the least-bound $v = 62$ state in ground state Sr_2 . Points denote experimentally measured ac polarizabilities at $\lambda = 1.95 \mu\text{m}$. Lines are *ab initio* polarizabilities from dc to $\lambda = 1.25 \mu\text{m}$.

TABLE I. Investigated $^{88}\text{Sr}_2$ molecular states. The initial state is always the rotationless top $v' = 62$ level; v denotes the target level in the $^1\text{S}_0 + ^1\text{S}_0 0_g^+$ ground state and λ_{magic} is the magic wavelength. The differential polarizabilities are expressed in atomic units of $e^2 a_0^2 / E_h$, where e is the electron charge, a_0 is the Bohr radius and E_h is the Hartree energy [52]. The error bars on theoretical polarizabilities stem from comparison to experiment.

Clock transitions		Differential polarizability $\alpha_{v \leftrightarrow v'}(\omega)$ (a.u.)						
$X 0_g^+ v \leftrightarrow v'$	v''	$f_{v \leftrightarrow v'}$ (MHz)	\tilde{R}_v (a.u.)	λ_{magic} (nm)	Exp. (1.95 μm)	Th. (1.95 μm)	Th. (dc)	$\Delta f_{v \leftrightarrow v'}$ (Hz)
$61 \leftrightarrow 62$	15	1263.673 58(20) [45]	43.6	—	-0.41(0.52)	-0.1326(35)	-0.1080(28)	$+9.32(25) \times 10^{-4}$
$55 \leftrightarrow 62$	15	108 214.221(10)	21.6	—	-3.68(0.38)	-2.985(78)	-2.429(63)	+0.020 99(56)
$41 \leftrightarrow 62$	11	2 177 876.735(81)	13.6	996.4379(10)	-21.67(0.88)	-19.10(50)	-15.60(41)	+0.134 9(37)
$27 \leftrightarrow 62$	11	8 075 406.280(18)	11.1	1006.5787(10)	-40.4(1.8)	-39.3(1.0)	-31.99(84)	+0.276 8(75)
$12 \leftrightarrow 62$	16	19 176 451.651(35)	9.62	1007.7634(10)	-60.1(4.0)	-61.3(1.6)	-49.7(1.3)	+0.430(12)
$7 \leftrightarrow 62$	15	24 031 492.422(24)	9.27	1007.1334(10)	-66.0(2.5)	-68.3(1.8)	-55.1(1.4)	+0.477(13)
$1 \leftrightarrow 62$	11	30 640 159.753(75)	8.91	1016.9714(10)	-75.7(3.3)	-76.0(2.0)	-61.1(1.6)	+0.529(15)
$0 \leftrightarrow 62$	11	31 825 183.207 5928(51) [41]	8.86	1004.7720(10)	-76.4(3.6)	-77.2(2.0)	-62.1(1.7)	+0.538(15)

polarizabilities for all molecular clock transitions thusly: first, we calculate *ab initio* electronic polarizabilities of the strontium dimer as a function of internuclear distance R , and second, we obtain the polarizability for each vibrational level as an average of the electronic polarizability over the vibrational wavefunction.

In homonuclear molecules only electronic transitions contribute to polarizabilities and BBR shifts. To calculate the electronic polarizability, we employ the approach based on asymmetric analytical derivative of the coupled-cluster energy with single and double excitations (CCSD) [59], as

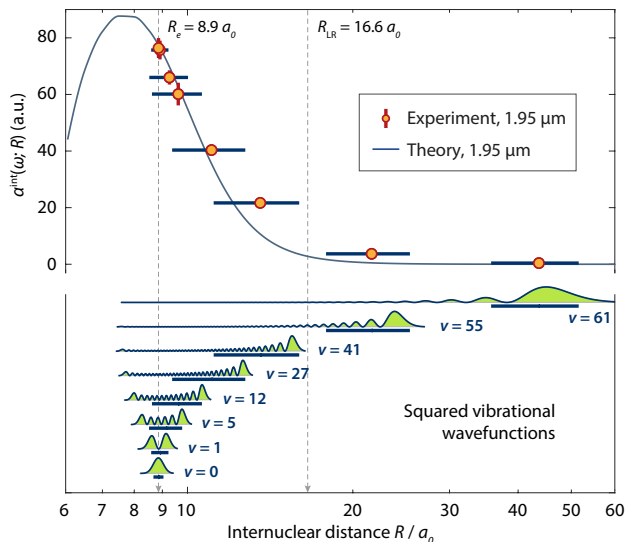


FIG. 3. Interaction-induced ac polarizability at $\lambda = 1.95 \mu\text{m}$. In addition to the *ab initio* result we show absolute experimental polarizabilities in relation to mean internuclear distances \tilde{R} (Table I). Horizontal bars indicate the range $[\tilde{R}_v - S_{R_v}, \tilde{R}_v + S_{R_v}]$ of internuclear distances probed by the vibrational wavefunctions shown in the lower panel. Here \tilde{R}_v and S_{R_v} are the mean and standard deviation internuclear distances for wavefunction squared treated as a probability distribution. R_e and R_{LR} are the equilibrium distance and the LeRoy radius [57, 58].

implemented in the Q-Chem 5 package [60]. We use the ECP28MDF pseudopotential and its dedicated valence basis set [61].

For any given light frequency ω , we first calculate the molecular interaction-induced polarizability, $\alpha_{ij}^{\text{int}}(\omega; R) = \alpha_{ij}(\omega; R) - 2\alpha_{\text{atom}}(\omega)$, where $\alpha_{ij}(\omega)$ are tensor components of the total molecular polarizability and $\alpha_{\text{atom}}(\omega)$ is the atomic polarizability at frequency ω . Since we only use isotropic $J = 0$ states, we take the trace polarizability $\alpha^{\text{int}}(\omega; R) = [\alpha_{zz}^{\text{int}}(\omega; R) + 2\alpha_{xx}^{\text{int}}(\omega; R)]/3$ [62, 63]. We extend the model for large R using a fitted long-range form $\alpha^{\text{int}}(\omega; R) \sim A_6(\omega)R^{-6} + A_8(\omega)R^{-8} + A_{10}(\omega)R^{-10}$ [64]. Figure 3 shows the isotropic component $\alpha^{\text{int}}(\omega; R)$ at 1.95 μm as a function of R .

Secondly, we calculate the polarizability of each vibrational level v by averaging the electronic polarizability $\alpha^{\text{int}}(R)$ over the level's vibrational wavefunction $\Psi_v(R)$:

$$\alpha_v^{\text{int}}(\omega) = \int_0^\infty |\Psi_v(R)|^2 \alpha^{\text{int}}(\omega; R) dR \quad (1)$$

where the differential polarizability for a transition $v \leftrightarrow v'$ is

$$\Delta\alpha_{v \leftrightarrow v'}(\omega) = \alpha_v^{\text{int}}(\omega) - \alpha_{v'}^{\text{int}}(\omega). \quad (2)$$

We obtain the vibrational wavefunctions by solving the Schrödinger equation, $[-(\hbar^2/2\mu)(d^2/dR^2) + V(R)]\Psi_v(R) = E_v\Psi_v(R)$, using a matrix method [65, 66]. We use an empirical molecular potential $V(R)$ [67]; the reduced mass μ equals half the mass of a Sr atom. The uncertainties of the potential curve are negligible for our purposes (Supplemental Material). Figure 2 shows calculated differential dc and ac polarizabilities for $v \leftrightarrow 62$ transitions. It is noteworthy that this approach is valid only when the adiabaticity condition is maintained, that is, that the ground-state potential does not cross any of the excited-state potentials if shifted upwards by the energy of the incident photon. In Sr_2 , this limits the photon wavenumber to about 8000 cm^{-1} ($1.25 \mu\text{m}$). Both our 1.95- μm (5128 cm^{-1}) laser and room-temperature BBR are well within this margin.

We first validate the *ab initio* model using polarizabilities of the ground-state Sr atom. At dc we find a polarizability of

+197.327 a.u., in excellent agreement with the state-of-the-art semi-empirical value of +197.14(20) a.u. [40]. Similarly, our ac polarizability of +207.524 a.u. at 1.95 μm agrees perfectly with the value of +208.2(1.1) a.u. [55].

The key test of our model is the direct comparison and strong agreement of measured differential polarizability at 1.95 μm with the calculated values (Figure 2). For example, the theoretical differential polarizability for the $0 \leftrightarrow 62$ clock transition, $\Delta\alpha_{0 \leftrightarrow 62}(\omega) = -77.2$ a.u. compares well to the experimental $-76.4(3.6)$ a.u. Moving to more weakly bound target states, the differential polarizabilities decrease monotonically. We elucidate this using the R -centroid approximation [68] and the concept of a LeRoy radius R_{LR} [57, 58]. Firstly, the R -centroid approximation allows us to estimate the interaction-induced polarizability at the mean internuclear distance \tilde{R}_ν of state ν using the differential polarizability of a $\nu \leftrightarrow 62$ transition:

$$\alpha^{\text{int}}(\omega; \tilde{R}_\nu) \approx -\Delta\alpha_{\nu \leftrightarrow 62}(\omega), \quad (3)$$

where $\tilde{R}_\nu = \int_0^\infty |\Psi_\nu(R)|^2 R dR$. We neglect the small interaction-induced polarizability of the $\nu' = 62$ state. Thus, different vibrational transitions effectively serve as probes of polarizabilities, each at a different internuclear separation (Figure 3).

The range of investigated target levels from the ground $\nu = 0$ to the second-to-least bound $\nu = 61$ states spans internuclear distances from $8.86 a_0$ (approximately the equilibrium distance R_e) to $43.6 a_0$. Beyond the LeRoy radius $R_{LR} = 16.6 a_0$ the interaction-induced polarizability is negligible: Sr_2 becomes a “physicist’s molecule” [48] whose polarizability is that of two strontium atoms. At shorter internuclear separations, it becomes a “chemist’s molecule” and picks up over 80 a.u. of extra polarizability due to molecular bonding of the two constituent atoms. The qualitative boundary between the two extremes is set by $R_{LR} = 2(r_A + r_B)$ where $r_A = r_B = 4.15 a_0$ are the RMS charge radii of the two atoms [69]. By selecting vibrational levels with different mean internuclear distances, we scan the interaction-induced polarizabilities at different internuclear separations, interpolating between the two extremes of “chemist’s” and “physicist’s” molecules.

To estimate the relative uncertainty of our theoretical model, we fit it to the experimental data by simple scaling. The best least-squares fit is achieved by scaling the model up by +1.8(2.4)%. This is compatible with zero, showing that no model scaling is necessary; in fact, the reduced chi-square $\chi^2/\text{dof} = 1.78$ for the scaled model (dof = 7) is worse than $\chi^2/\text{dof} = 1.69$ (dof = 8) for the original unscaled model. Thus, our *ab initio* model for the molecular polarizability contains no free parameters, justifying its use for all photon wavelengths. Out of caution, we combine the 2.4% uncertainty from the scaling factor with an additional 1.8% possible systematic error to obtain a “Type B” uncertainty [70] of 2.6%.

Finally, we calculate the BBR shift $\Delta f_{\nu \leftrightarrow \nu'}$ by integrating

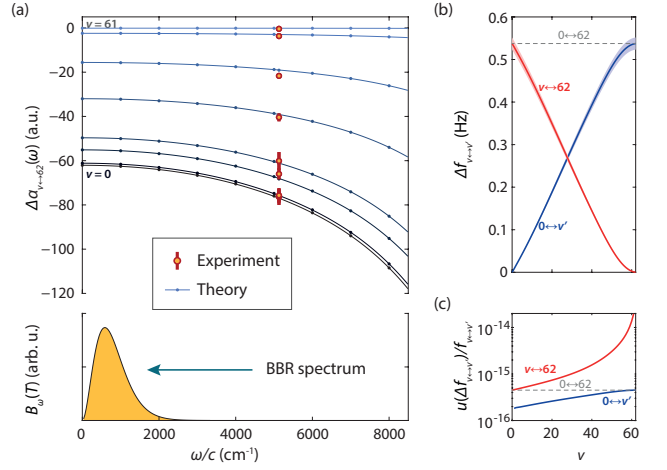


FIG. 4. (a) Differential polarizabilities in selected clock transitions. Below, a plot of a BBR spectral radiance $B_\omega(T)$ at 300 K. (b) Absolute BBR shift for $0 \leftrightarrow \nu'$ clock transitions. (c) Relative BBR uncertainty in same clock configurations.

the ac Stark shift over the BBR spectrum [37, 39, 71]:

$$\Delta f_{\nu \leftrightarrow \nu'} = -\frac{1}{2h} \int_0^\infty \frac{4\pi}{\epsilon_0 c} B_\omega(T) \Delta\alpha_{\nu \leftrightarrow \nu'}(\omega) d\omega. \quad (4)$$

The BBR spectral radiance at temperature T is

$$B_\omega(T) = \frac{\hbar\omega^3}{4\pi^3 c^2} \frac{1}{\exp(\hbar\omega/k_B T) - 1}. \quad (5)$$

Typically, BBR shifts for atomic clocks are determined using sum-over-states to calculate the static and dynamic terms [37, 38, 40, 71, 72], but we already have computed the dynamic polarizabilities. We can directly integrate the BBR shift. Since practically all of the BBR spectrum falls below any resonance frequencies in our system, we expand the polarizability using Cauchy coefficients [72]: $\Delta\alpha_{\nu \leftrightarrow \nu'}(\omega) = \Delta\alpha_{\nu \leftrightarrow \nu'}^{(0)} + \Delta\alpha_{\nu \leftrightarrow \nu'}^{(2)}\omega^2 + \Delta\alpha_{\nu \leftrightarrow \nu'}^{(4)}\omega^4 + \dots$ that we fit to tenth order to numerical polarizabilities [Fig. 4(a)]. This allows expressing the BBR shift as a series:

$$\Delta f_{\nu \leftrightarrow \nu'} = \sum_{n=0,2,\dots} \Delta f_\nu^{(n)} = \sum_{n=0,2,\dots} -\frac{c_n \Delta\alpha_{\nu \leftrightarrow \nu'}^{(n)}}{4\pi^3 \epsilon_0 c^3} \left(\frac{k_B T}{\hbar}\right)^{4+n}, \quad (6)$$

where the Planck integrals $c_n = \int_0^\infty u^{3+n}/(e^u - 1) du$ appear in Table II (Supplemental Material). The leading term is the well known static contribution [39, 40], while further terms constitute a dynamic correction η on the order of 0.5–0.6% (Table II). Here, terms beyond the second order are negligible.

Since the molecular clock uniquely provides an array of available clock states, we calculate the BBR shift for other clock transitions. In Fig. 4(b), we plot the BBR shift for $\nu \leftrightarrow 62$ transitions, $\Delta f_{\nu \leftrightarrow 62}$ (red line). For our previously measured clock transition [41] $\Delta f_{0 \leftrightarrow 62} = +538(15)$ mHz, giving a BBR contribution to fractional uncertainty of $u(\Delta f_{\nu \leftrightarrow \nu'})/f_{\nu \leftrightarrow \nu'} = 4.7 \times 10^{-16}$. Further, the BBR contribution to fractional uncertainty of the molecular clock transition can be reduced by

TABLE II. Contributions to the BBR shift at 300 K for the $0 \leftrightarrow 1$ and $0 \leftrightarrow 62$ transitions.

n	c_n	$\Delta f_{0 \leftrightarrow 1}^{(n)}$ (Hz)	$\Delta f_{0 \leftrightarrow 1}^{(n)}/f_{0 \leftrightarrow 1}$	$\Delta f_{0 \leftrightarrow 62}^{(n)}$ (Hz)	$\Delta f_{0 \leftrightarrow 62}^{(n)}/f_{0 \leftrightarrow 62}$
0	$\pi^4/15$	+0.0081	$+6.8 \times 10^{-15}$	+0.53	$+1.7 \times 10^{-14}$
2	$8\pi^6/63$	$+6.1 \times 10^{-5}$	$+5.1 \times 10^{-17}$	+0.0033	$+1.0 \times 10^{-16}$
4	$8\pi^8/15$	$+6.5 \times 10^{-7}$	$+5.5 \times 10^{-19}$	$+6.3 \times 10^{-5}$	$+2.0 \times 10^{-18}$
η (%)			0.54		0.62

handpicking $0 \leftrightarrow \nu'$ clock transitions (blue line) between deeply bound vibrational states [Fig. 4(c)]. This configuration could allow fractional uncertainties as low as 1.8×10^{-16} , a factor of ~ 2.5 lower than the $0 \leftrightarrow 62$ transition.

Clock transitions between deeply bound states could allow magic wavelengths further detuned from excited molecular resonances due to a smaller polarizability gap to overcome. That could improve molecular trap lifetimes and Q-factors. These can also be improved by switching to vertical lattice geometry. Conversely, this requires the use of STIRAP [43, 73, 74] to initialize the molecule population in a deeply bound state, increasing experimental complexity.

In the future, our technique can be pushed further. The polarizability measurement relies on frequency shifts that could be determined at the full Hz-level clock accuracy. It also depends on semiempirical atomic polarizabilities that currently contribute about 10% of the error bar. However, with better measurements, the *ab initio* model will cease to agree with experiment. Scaling is an option, but a complementary approach is possible where polarizabilities are measured at different wavelengths and Cauchy coefficients are instead fitted to experiment.

In conclusion, we have determined the BBR shift in a strontium molecular lattice clock. We leveraged agreement between precision spectroscopy and modern quantum chemistry to provide a robust description of the polarizabilities of ground state Sr_2 molecules. Specifically, we performed ac Stark shift spectroscopy of several molecular clock transitions throughout the ground state potential induced by an additional mid-infrared laser. These measurements were in excellent agreement with *ab initio* calculations of molecular polarizability, lending credence to extending this model to other wavelengths. This determination will allow us to control the BBR shift systematic to the 10^{-16} level. Selecting a clock transition between deeply bound vibrational states ($\nu < 10$) could further suppress the BBR effect. Additional measurements of ac or dc Stark shifts, such as by direct application of an electric field [37] or with a CO_2 laser [75, 76], could further constrain the theoretical model and improve control of the BBR systematic. A next-generation molecular clock could search for new interactions beyond the Standard Model or probe the variations of fundamental constants. This work paves the way towards mHz-level spectroscopy in Sr_2 molecules.

We thank M. Safronova for providing theoretical atomic polarizabilities, P. S. Żuchowski for fruitful discussions,

I. Majewska for involvement and discussions at the early stages of this project and J. Dai, D. Mitra and Q. Sun for experimental assistance. This work was supported by NSF grant PHY-1911959, AFOSR MURI FA9550-21-1-0069, ONR grant N00014-21-1-2644, the Brown Science Foundation, and the Polish National Science Centre (NCN) grant 2016/21/B/ST4/03877. M. B. was partially funded by the Polish National Agency for Academic Exchange within the Bekker Programme, project PPN/BEK/2020/1/00306/U/00001, and by NCN, grant 2017/25/B/ST4/01486. W.S. acknowledges Polish high-performance computing infrastructure PLGrid (HPC Centers: ACK Cyfronet AGH) for providing computer facilities and support within computational grant no. PLG/2022/015675.

* These authors contributed equally to this work.

† mateusz@cold-molecules.com

‡ tanya.zelevinsky@columbia.edu

- [1] M. Takamoto, F.-L. Hong, R. Higashi, and H. Katori, An optical lattice clock, *Nature* **435**, 321 (2005).
- [2] H. Katori, Optical lattice clocks and quantum metrology, *Nature Photonics* **5**, 203 (2011).
- [3] W. F. McGrew, X. Zhang, R. J. Fasano, S. A. Schäffer, K. Beloy, D. Nicolodi, R. C. Brown, N. Hinkley, G. Milani, M. Schioppo, T. H. Yoon, and A. D. Ludlow, Atomic clock performance enabling geodesy below the centimetre level, *Nature* **564**, 87 (2018).
- [4] T. Bothwell, D. Kedar, E. Oelker, J. M. Robinson, S. L. Bromley, W. L. Tew, J. Ye, and C. J. Kennedy, JILA SrI optical lattice clock with uncertainty of 2×10^{-18} , *Metrologia* **56**, 065004 (2019).
- [5] W. F. McGrew, X. Zhang, H. Leopardi, R. J. Fasano, D. Nicolodi, K. Beloy, J. Yao, J. A. Sherman, S. A. Schäffer, J. Savory, R. C. Brown, S. Römisch, C. W. Oates, T. E. Parker, T. M. Fortier, and A. D. Ludlow, Towards the optical second: verifying optical clocks at the SI limit, *Optica* **6**, 448 (2019).
- [6] J. Lodewyck, On a definition of the si second with a set of optical clock transitions, *Metrologia* **56**, 055009 (2019).
- [7] S. Bize, The unit of time: Present and future directions, *Comptes Rendus Physique* **20**, 153 (2019).
- [8] M. Borkowski, Optical Lattice Clocks with Weakly Bound Molecules, *Physical Review Letters* **120**, 083202 (2018).
- [9] S. S. Kondov, C.-H. Lee, K. H. Leung, C. Liedl, I. Majewska, R. Moszynski, and T. Zelevinsky, Molecular lattice clock with long vibrational coherence, *Nature Physics* **15**, 1118 (2019).
- [10] J. Kobayashi, A. Ogino, and S. Inouye, Measurement of the variation of electron-to-proton mass ratio using ultracold molecules produced from laser-cooled atoms, *Nature Communications* **10**, 3771 (2019).
- [11] D. Hanneke, B. Kuzhan, and A. Lunstad, Optical clocks based on molecular vibrations as probes of variation of the proton-to-electron mass ratio, *Quantum Science and Technology* **6**, 014005 (2020).
- [12] G. Barontini, L. Blackburn, V. Boyer, F. Butuc-Mayer, X. Calmet, J. R. Crespo López-Urrutia, E. A. Curtis, B. Darquié, J. Dunningham, N. J. Fitch, E. M. Forgan, K. Georgiou, P. Gill, R. M. Godun, J. Goldwin, *et al.*, Measuring the stability of fundamental constants with a network of clocks, *EPJ Quantum*

- Technology **9**, 12 (2022).
- [13] E. J. Salumbides, W. Ubachs, and V. I. Korobov, Bounds on fifth forces at the sub-Å length scale, *Journal of Molecular Spectroscopy* **300**, 65 (2014).
- [14] J. Biesheuvel, J.-P. Karr, L. Hilico, K. Eikema, W. Ubachs, and J. Koelmeij, Probing QED and fundamental constants through laser spectroscopy of vibrational transitions in HD⁺, *Nature Communications* **7**, 10385 (2016).
- [15] M. Borkowski, A. A. Buchachenko, R. Ciuryło, P. S. Julienne, H. Yamada, Y. Kikuchi, Y. Takasu, and Y. Takahashi, Weakly bound molecules as sensors of new gravitylike forces, *Scientific Reports* **9**, 14807 (2019).
- [16] B. Heacock, T. Fujii, R. W. Haun, A. Henins, K. Hirota, T. Hosobata, M. G. Huber, M. Kitaguchi, D. A. Pushin, H. Shimizu, M. Takeda, R. Valdillez, Y. Yamagata, and A. R. Young, Pendellösung interferometry probes the neutron charge radius, lattice dynamics, and fifth forces, *Science* **373**, 1239 (2021).
- [17] S. Schiller and V. Korobov, Tests of time independence of the electron and nuclear masses with ultracold molecules, *Phys. Rev. A* **71**, 032505 (2005).
- [18] D. DeMille, S. Sainis, J. Sage, T. Bergeman, S. Kotochigova, and E. Tiesinga, Enhanced sensitivity to variation of m_e/m_p in molecular spectra, *Physical Review Letters* **100**, 043202 (2008).
- [19] K. Beloy, A. W. Hauser, A. Borschevsky, V. V. Flambaum, and P. Schwerdtfeger, Effect of Alpha variation on the vibrational spectrum of Sr₂, *Phys. Rev. A* **84**, 062114 (2011).
- [20] S. Schiller, D. Bakalov, and V. I. Korobov, Simplest molecules as candidates for precise optical clocks, *Phys. Rev. Lett.* **113**, 023004 (2014).
- [21] M. Kajita, G. Gopakumar, M. Abe, M. Hada, and M. Keller, Test of m_p/m_e changes using vibrational transitions in n₂⁺, *Phys. Rev. A* **89**, 032509 (2014).
- [22] M. Germann, X. Tong, and S. Willitsch, Observation of electric-dipole-forbidden infrared transitions in cold molecular ions, *Nature Physics* **10**, 820 (2014).
- [23] P. Wcisło, P. Ablewski, K. Beloy, S. Bilicki, M. Bober, R. Brown, R. Fasano, R. Ciuryło, H. Hachisu, T. Ido, J. Lodewyck, A. Ludlow, W. McGrew, P. Morzyński, D. Nicolodi, M. Schioppo, M. Sekido, R. Le Targat, P. Wolf, X. Zhang, B. Zjawin, and M. Zawada, New bounds on dark matter coupling from a global network of optical atomic clocks, *Science Advances* **4**, eaau4869 (2018).
- [24] M. S. Safronova, The search for variation of fundamental constants with clocks, *Annalen der Physik* **531**, 1800364 (2019).
- [25] N. R. Hutzler, Polyatomic molecules as quantum sensors for fundamental physics, *Quantum Science and Technology* **5**, 044011 (2020).
- [26] R. Lange, N. Huntemann, J. M. Rahm, C. Sanner, H. Shao, B. Lipphardt, C. Tamm, S. Weyers, and E. Peik, Improved limits for violations of local position invariance from atomic clock comparisons, *Phys. Rev. Lett.* **126**, 011102 (2021).
- [27] R. Le Targat, L. Lorini, Y. Le Coq, M. Zawada, J. Guéna, M. Abgrall, M. Gurov, P. Rosenbusch, D. G. Rovera, B. Nagórny, R. Gartman, P. G. Westergaard, M. E. Tobar, M. Lours, G. Santarelli, A. Clairon, S. Bize, P. Laurent, P. Lemonde, and J. Lodewyck, Experimental realization of an optical second with strontium lattice clocks, *Nature Communications* **4**, 2109 (2013).
- [28] S. Falke, N. Lemke, C. Grebing, B. Lipphardt, S. Weyers, V. Gerginov, N. Huntemann, C. Hagemann, A. Al-Masoudi, S. Häfner, S. Vogt, U. Sterr, and C. Lisdat, A strontium lattice clock with 3×10^{-17} inaccuracy and its frequency, *New Journal of Physics* **16**, 073023 (2014).
- [29] T. Nicholson, S. Campbell, R. Hutson, G. Marti, B. Bloom, R. McNally, W. Zhang, M. Barrett, M. Safronova, G. Strouse, W. Tew, and J. Ye, Systematic evaluation of an atomic clock at 2×10^{-18} total uncertainty, *Nature Communications* **6**, 6896 (2015).
- [30] S. B. Koller, J. Grotti, S. Vogt, A. Al-Masoudi, S. Dörscher, S. Häfner, U. Sterr, and C. Lisdat, Transportable optical lattice clock with 7×10^{-17} uncertainty, *Phys. Rev. Lett.* **118**, 073601 (2017).
- [31] Y. Hisai, D. Akamatsu, T. Kobayashi, K. Hosaka, H. Inaba, F.-L. Hong, and M. Yasuda, Improved frequency ratio measurement with ⁸⁷Sr and ¹⁷¹Yb optical lattice clocks at NMIJ, *Metrologia* **58**, 015008 (2021).
- [32] N. Ohmae, M. Takamoto, Y. Takahashi, M. Kokubun, K. Araki, A. Hinton, I. Ushijima, T. Muramatsu, T. Furumiya, Y. Sakai, N. Moriya, N. Kamiya, K. Fujii, R. Muramatsu, T. Shiimado, and H. Katori, Transportable Strontium Optical Lattice Clocks Operated Outside Laboratory at the Level of 10^{-18} Uncertainty, *Advanced Quantum Technologies* **4**, 2100015 (2021).
- [33] I. Ushijima, M. Takamoto, M. Das, T. Ohkubo, and H. Katori, Cryogenic optical lattice clocks, *Nature Photonics* **9**, 185 (2015).
- [34] P. Ablewski, M. Bober, and M. Zawada, Emissivities of vacuum compatible materials: towards minimising blackbody radiation shift uncertainty in optical atomic clocks at room temperatures, *Metrologia* **57**, 035004 (2020).
- [35] V. I. Yudin, A. V. Taichenachev, M. Y. BasalaeV, O. N. Prudnikov, H. A. Fürst, T. E. Mehlstäubler, and S. N. Bagayev, Combined atomic clock with blackbody-radiation-shift-induced instability below 10^{-19} under natural environment conditions, *New Journal of Physics* **23**, 023032 (2021).
- [36] T. Middelmann, C. Lisdat, S. Falke, J. S. R. Vellore Winfred, F. Riehle, and U. Sterr, Tackling the blackbody shift in a strontium optical lattice clock, *IEEE Transactions on Instrumentation and Measurement* **60**, 2550 (2011).
- [37] T. Middelmann, S. Falke, C. Lisdat, and U. Sterr, High accuracy correction of blackbody radiation shift in an optical lattice clock, *Phys. Rev. Lett.* **109**, 263004 (2012).
- [38] C. Lisdat, S. Dörscher, I. Nosske, and U. Sterr, Blackbody radiation shift in strontium lattice clocks revisited, *Phys. Rev. Res.* **3**, L042036 (2021).
- [39] S. G. Porsev and A. Derevianko, Multipolar theory of blackbody radiation shift of atomic energy levels and its implications for optical lattice clocks, *Phys. Rev. A* **74**, 020502 (2006).
- [40] M. S. Safronova, S. G. Porsev, U. I. Safronova, M. G. Kozlov, and C. W. Clark, Blackbody-radiation shift in the Sr optical atomic clock, *Physical Review A* **87**, 012509 (2013).
- [41] K. H. Leung, B. Iritani, E. Tiberi, I. Majewska, M. Borkowski, R. Moszynski, and T. Zelevinsky, Terahertz vibrational molecular clock with systematic uncertainty at the 10^{-14} level, *Phys. Rev. X* **13**, 011047 (2023).
- [42] K. H. Leung, I. Majewska, H. Bekker, C.-H. Lee, E. Tiberi, S. S. Kondov, R. Moszynski, and T. Zelevinsky, Transition strength measurements to guide magic wavelength selection in optically trapped molecules, *Phys. Rev. Lett.* **125**, 153001 (2020).
- [43] K. H. Leung, E. Tiberi, B. Iritani, I. Majewska, R. Moszynski, and T. Zelevinsky, Ultracold ⁸⁸Sr₂ molecules in the absolute ground state, *New Journal of Physics* **23**, 115002 (2021).
- [44] T. Zelevinsky, M. M. Boyd, A. D. Ludlow, T. Ido, J. Ye, R. Ciuryło, P. Naidon, and P. S. Julienne, Narrow Line Photoassociation in an Optical Lattice, *Physical Review Letters* **96**, 203201 (2006).
- [45] B. H. McGuyer, M. McDonald, G. Z. Iwata, M. G. Tarallo, A. T. Grier, F. Apfelbeck, and T. Zelevinsky, High-precision

- spectroscopy of ultracold molecules in an optical lattice, *New J. Phys* **17**, 055004 (2015).
- [46] S. H. Autler and C. H. Townes, Stark effect in rapidly varying fields, *Phys. Rev.* **100**, 703 (1955).
- [47] C. H. Townes and A. L. Schawlow, *Microwave spectroscopy* (Dover Publications, 1975).
- [48] K. M. Jones, E. Tiesinga, P. D. Lett, and P. S. Julienne, Ultracold photoassociation spectroscopy: Long-range molecules and atomic scattering, *Reviews of Modern Physics* **78**, 483 (2006).
- [49] Y. N. Martinez de Escobar, P. G. Mickelson, P. Pellegrini, S. B. Nagel, A. Traverso, M. Yan, R. Côté, and T. C. Killian, Two-photon photoassociative spectroscopy of ultracold ^{88}Sr , *Phys. Rev. A* **78**, 062708 (2008).
- [50] M. Kitagawa, K. Enomoto, K. Kasa, Y. Takahashi, R. Ciuryło, P. Naidon, and P. S. Julienne, Two-color photoassociation spectroscopy of ytterbium atoms and the precise determinations of s-wave scattering lengths, *Physical Review A* **77**, 012719 (2008).
- [51] See Supplemental Material for the determination of magic wavelengths and measurements of line positions, which includes Refs. [77–79].
- [52] E. Tiesinga, P. J. Mohr, D. B. Newell, and B. N. Taylor, Codata recommended values of the fundamental physical constants: 2018, *Rev. Mod. Phys.* **93**, 025010 (2021).
- [53] R. V. Pound, Electronic frequency stabilization of microwave oscillators, *Review of Scientific Instruments* **17**, 490 (1946).
- [54] R. W. Drever, J. L. Hall, F. V. Kowalski, J. Hough, G. Ford, A. Munley, and H. Ward, Laser phase and frequency stabilization using an optical resonator, *Applied Physics B* **31**, 97 (1983).
- [55] M. S. Safronova, private communication (2023).
- [56] M. McDonald, B. H. McGuyer, G. Z. Iwata, and T. Zelevinsky, Thermometry via light shifts in optical lattices, *Phys. Rev. Lett.* **114**, 023001 (2015).
- [57] R. J. Le Roy and R. B. Bernstein, Dissociation Energy and Long-Range Potential of Diatomic Molecules from Vibrational Spacings of Higher Levels, *The Journal of Chemical Physics* **52**, 3869 (1970).
- [58] R. J. Le Roy, *Molecular Spectroscopy - Volume I, A Specialist Periodical Report of the Chemical Society* (The Chemical Society, London, 1973) pp. 113–171.
- [59] K. D. Nanda and A. I. Krylov, Static polarizabilities for excited states within the spin-conserving and spin-flipping equation-of-motion coupled-cluster singles and doubles formalism: Theory, implementation, and benchmarks, *The Journal of Chemical Physics* **145**, 204116 (2016).
- [60] E. Epifanovsky, A. T. B. Gilbert, X. Feng, J. Lee, Y. Mao, N. Mardirossian, P. Pokhilko, A. F. White, M. P. Coons, A. L. Dempwolff, Z. Gan, D. Hait, P. R. Horn, L. D. Jacobson, I. Kaliman, *et al.*, Software for the frontiers of quantum chemistry: An overview of developments in the Q-Chem 5 package, *The Journal of Chemical Physics* **155**, 084801 (2021).
- [61] I. S. Lim, H. Stoll, and P. Schwerdtfeger, Relativistic small-core energy-consistent pseudopotentials for the alkaline-earth elements from Ca to Ra, *The Journal of Chemical Physics* **124**, 034107 (2006).
- [62] A. Dalgarno, A. L. Ford, and J. C. Browne, Direct Sum-of-States Calculations of the Frequency-Dependent Polarizability of H_2 , *Physical Review Letters* **27**, 1033 (1971).
- [63] J. M. Brown and A. Carrington, *Rotational Spectroscopy of Diatomic Molecules* (Cambridge University Press, Cambridge, 2003).
- [64] T. G. A. Heijmen, R. Moszynski, P. E. S. Wormer, and A. van der Avoird, Symmetry-adapted perturbation theory applied to interaction-induced properties of collisional complexes, *Molecular Physics* **89**, 81 (1996).
- [65] D. T. Colbert and W. H. Miller, A novel discrete variable representation for quantum mechanical reactive scattering via the S-matrix Kohn method, *J. Chem. Phys.* **96**, 1982 (1992).
- [66] E. Tiesinga, C. J. Williams, and P. S. Julienne, Photoassociative spectroscopy of highly excited vibrational levels of alkali-metal dimers: Green-function approach for eigenvalue solvers, *Phys. Rev. A* **57**, 4257 (1998).
- [67] A. Stein, H. Knöckel, and E. Tiemann, $^1\text{S}+^1\text{S}$ asymptote of Sr_2 studied by Fourier-transform spectroscopy, *Eur. Phys. J. D* **57**, 171 (2010).
- [68] P. A. Fraser, A method of determining the electronic transition moment for diatomic molecules, *Canadian Journal of Physics* **32**, 515 (1954).
- [69] E. Clementi, D. L. Raimondi, and W. P. Reinhardt, Atomic Screening Constants from SCF Functions. II. Atoms with 37 to 86 Electrons, *J. Chem. Phys.* **471**, 1300 (1967).
- [70] B. N. Taylor and C. E. Kuyatt, *NIST Technical Note 1297. Guidelines for evaluating and expressing the uncertainty of NIST measurement results* (US Department of Commerce, Technology Administration, National Institute of Standards and Technology, 1994).
- [71] J. W. Farley and W. H. Wing, Accurate calculation of dynamic stark shifts and depopulation rates of Rydberg energy levels induced by blackbody radiation. Hydrogen, helium, and alkali-metal atoms, *Phys. Rev. A* **23**, 2397 (1981).
- [72] J. Mitroy, M. S. Safronova, and C. W. Clark, Theory and applications of atomic and ionic polarizabilities, *Journal of Physics B: Atomic, Molecular and Optical Physics* **43**, 202001 (2010).
- [73] K. Bergmann, H. Theuer, and B. W. Shore, Coherent population transfer among quantum states of atoms and molecules, *Reviews of Modern Physics* **70**, 1003 (1998).
- [74] N. V. Vitanov, A. A. Rangelov, B. W. Shore, and K. Bergmann, Stimulated Raman adiabatic passage in physics, chemistry, and beyond, *Reviews of Modern Physics* **89**, 1 (2017).
- [75] J. Chen, To simulate blackbody radiation frequency shift in cesium fountain frequency standard with CO_2 laser, *IEEE Transactions on Ultrasonics, Ferroelectrics and Frequency Control* **53**, 1685 (2006).
- [76] K. J. Arnold, R. Kaewuam, A. Roy, T. R. Tan, and M. D. Barrett, Blackbody radiation shift assessment for a lutetium ion clock, *Nature Communications* **9**, 1650 (2018).
- [77] K. D. Bonin and V. V. Kresin, *Electric-dipole polarizabilities of atoms, molecules, and clusters* (World Scientific, 1997).
- [78] L. Landau and E. Lifshitz, *Statistical Physics* (Pergamon Press, 1958).
- [79] R. J. Le Roy, N. S. Dattani, J. A. Coxon, A. J. Ross, P. Crozet, and C. Linton, Accurate analytic potentials for $\text{Li}_2(\text{X } ^1\Sigma_g)$ and $\text{Li}_2(\text{A X } ^1\Sigma_u^+)$ from 2 to 90 Å, and the radiative lifetime of $\text{Li}(2p)$, *The Journal of Chemical Physics* **131**, 204309 (2009).